Ionics (2022) 28:4547–4554
https://doi.org/10.1007/s11581-022-04691-4

ORIGINAL PAPER

Enhanced cyclic stability of $LiNi_{0.8}Co_{0.1}Mn_{0.1}O_2$ (NCM811) by AlF_3 coating via atomic layer deposition

Chengsheng Yang[1] · Yuyu Li[1] · Xuanxuan Zhang[2] · Jingjing Xiao[3] · Hongbo Xiong[3] · Weizhe Li[4] · Pingmei Guo[1] · Zehui Yang[5] · Ming Xie[1]

Received: 10 March 2022 / Revised: 11 July 2022 / Accepted: 18 July 2022 / Published online: 2 August 2022

Abstract
$LiNi_{0.8}Co_{0.1}Mn_{0.1}O_2$ (NCM811) is a promising cathode material for lithium-ion batteries due to its high energy density and low cost. However, NCM811 suffers from poor cycling stability and storage sensitivity to air and moisture. This study introduces an AlF_3 protective layer onto the surface of NCM811 (NCM811-AlF_3) by atomic layer deposition (ALD). After the AlF_3 layer protection, the initial capacity of the quasi-solid-state pouch cell with the NCM811 cathode was significantly increased from 148 to 180 mAh g^{-1}. In addition, NCM811-AlF_3 maintained a capacity of 167 mAh g^{-1}, which exceeded that of pristine NCM811 (126 mAh g^{-1}) after 500 cycles. This excellent electrochemical performance is attributed to the conformal AlF_3 protective layer that prevents the NCM811 from coming into direct contact with the electrolyte. In addition, the AlF_3 protective layer can prevent the Li/Ni mixture and Li loss during cycling by limiting the lattice expansion. Moreover, it can suppress the generation of residual alkali on the NCM811 surface during storage, improving the interfacial stability between NCM811 and the electrolytes. These results indicate that AlF_3 protective layer by ALD can be an effective method for improving the performance of high-energy–density cathode materials.

Keywords AlF_3 protective layer · Atomic layer deposition · NCM811 · Lithium-ion batteries

Introduction

Demands for higher energy density, longer cycle life, and better safety of lithium-ion batteries (LIBs) are increasing as the popularity of electric vehicles (EVs) and smart power grids grow [1–3]. Cathode materials are key components of LIBs. Therefore, improvements in state-of-the-art cathode materials are required for advanced LIBs [4].

Currently, a Ni-rich cathode material, $LiNi_xCo_yMn_{1-x-y}O_2$ (NCM) ($x \geq 0.5$), is considered a highly promising cathode material for LIBs due to its low cost and high capacity [5]. However, during the charging process, Ni^{2+} and Ni^{3+} cations are oxidized to a high valence state (Ni^{4+}) with strong reactivity, resulting in several parasitic reactions and continuous consumption of the electrolyte [6]. The cation mixing between Li^+ (0.76 Å) and Ni^{2+} (0.69 Å) causes the migration of transition metal ions to Li vacancies, which reconstructs the surface and then results in layered disordered spinel or rock salt generation on the surface of NCM811. These inactive phases increase the electrode's interfacial resistance and reduce the capacity. In addition, the low conductivity (10^{-3}–10^{-5} S cm^{-1}) of NCM811 limits the charge carrier migration, resulting in a high internal resistance [7]. Further, microcracks in NCM811 secondary particles are the accumulation of microsequences produced by c-axis expansion/contraction, resulting in rapid capacity degradation.

Several methods have been proposed to address these problems, including surface modification or coating,

✉ Yuyu Li
YuyuLi@jhun.edu.cn

✉ Ming Xie
ming.xie@jhun.edu.cn

1 Key Laboratory of Optoelectronic Chemical Materials and Devices of Ministry of Education, Jianghan University, Wuhan 430056, China

2 Ningbo Enerol Nanotechnology Co., Ltd, Ningbo 315000, China

3 BattFlex Technology Co., Ltd, Wuhan 430200, China

4 China Mobile Group Hubei Co., Ltd, Wuhan 430024, China

5 Sustainable Energy Laboratory, Faculty of Materials Science and Chemistry, China University of Geosciences Wuhan, Wuhan 430074, China

electrolyte additives, and cation doping [8–18]. Among them, the surface coating is an effective method for preparing core–shell structures of Ni-rich cathode materials, such as Al_2O_3, TiO_2, V_2O_5, Li_3PO_4, and Mn-rich shells [14–20]. These coating layers can prevent direct contact between a highly active cathode and electrolyte, inhibiting the parasitic reaction and the generation of microcracks to a certain extent. However, the metal oxide components have low stability with HF in the liquid electrolyte, which degrades the electrode's cyclic performance and rate capability. AlF_3 is a promising material for interfacial optimization due to its higher stability and wider bandgap (> 10 eV) than most metal oxides [21]. In addition, AlF_3 is stable with HF, allowing the AlF_3 protective layer to remain intact, which is beneficial for cyclic performance and rate capability of the electrode [22].

However, the traditional dry or wet coatings have minimal controllability on coating thickness and conformality [6]. Therefore, AlF_3 protective layers are commonly nonuniform and the AlF_3 layer is too thick, resulting in the impedance of the ionic and electronic transfer of electrodes [22]. Atomic layer deposition (ALD) is an advanced coating technology that can deposit uniform films on substrates with a high specific surface area, even with irregular geometry, and can precisely control its thickness [23]. Therefore, AlF_3 ALD coating is a promising method for interfacial optimization of the electrode. Zhou et al. reported freestanding $LiCoO_2$/multiwall carbon nanotube/nanocellulose fibril (LCO-MWCNT-NCF) coated with AlF_3 via ALD using TMA and HF-pyridine, which showed a high specific capacity of 216 mAh g^{-1} at 4.7 V [21]. A. Shapira et al. recently reported an ultrahigh-voltage cathode material, $LiMn_{1.5}Ni_{0.5}O_4$ (LMNO), coated with AlF_3, and the capacity retention of the AlF_3-coated LMNO significantly exceeded that of pristine LMNO [24]. Therefore, AlF_3 could be a promising protecting layer for improving NCM811 stability.

In this study, $LiNi_{0.8}Co_{0.1}Mn_{0.1}O_2$ (NCM811) with AlF_3 nanocoating was synthesized by ALD. The surficial compositions of NCM811 were characterized using X-ray diffraction (XRD), X-ray photoelectron spectroscopy (XPS), and transmission electron microscope (TEM). AlF_3 layer deposited by ALD can significantly promote the cycle and rate performance of NCM811 at 4.25 V in a half cell. The electrochemical performances of the pouch cell and gel-electrolyte LIBs were also significantly improved.

Experimental section

Material synthesis and preparation

Pristine NCM811 was provided by Hunan Shanshan. AlF_3 thin films were deposited directly on different amounts of NMC811 powder in an ALD reactor (YUNMAO, GM10) at BattFlex (Wuhan). The ALD process uses trimethylaluminium (TMA) (97%) and HF-pyridine as the following precursors were employed for the AlF_3 coating on the powder of NCM811 [25]:

$$(A) AlF_3 - HF^* + Al(CH_3)_3 \rightarrow AlF_3 - AlF(CH_3)_2^* + CH_4$$

$$(B) AlF\left(CH_3\right)_2^* + HF \rightarrow AlF_3 - HF^* + CH_4$$

The AlF_3 ALD reaction sequence is as follows [21]: (i) dose TMA to 2.0 Torr; (ii) keep TMA pressure constant for 30 s; (iii) evacuate reaction products and excess TMA for 60 s; (iv) flow 50 sccm N_2 for 360 s; (v) evacuate N_2 for 60 s; (vi) dose HF to 1.0 Torr; (vii) keep HF pressure constant for 30 s; (viii) evacuate reaction products and excess HF for 60 s; (ix) flow 50 sccm N_2 for 360 s; (x) evacuate N_2 for 60 s. This sequence constitutes one AB cycle of AlF_3 ALD, and repeat this cycle four times to get the material. The temperature of the two sources is 45 °C, and the AlF_3 ALD was conducted at 180 °C. NCM811 with AlF_3 is labeled NCM811-AlF_3.

Material characterizations

The morphologies of pristine NMC811 and NCM811-AlF_3 were observed by scanning electron microscopy (SEM) and TEM. Element mapping was performed by an energy dispersive X-ray spectrometer (EDX). XRD was conducted at $2\theta = 5° - 80°$ with Cu Kα radiation on a PANalytical X-ray diffractometer, and the crystal lattice parameters were refined using the General Structure Analysis Software (GSAS program). XPS was performed using an Mg Kα source (1253.6 eV) at 12 kV and 25 mA under a high vacuum pressure of 10^{-7} Pa at room temperature. All the binding energy values were referenced to the carbon peak C 1 s at 285.0 eV.

Electrochemical performance testing

The working electrodes were made by mixing the active materials with polyvinylidene fluoride and carbon black in a weight ratio of 80:10:10 in a 1-methyl-2-pyrrolidinone (NMP) solvent. The slurry was coated onto aluminum foil and dried at 100 °C for 24 h. The loading of the working electrode was nearly 3.2 mg cm^{-2}. A Celgard separator 2340 with a 1-M $LiPF_6$ electrolyte solution in a 1:1 w/w ethylene-carbonate:diethyl-carbonate (Novolyte) was used. The N/P of the pouch and quasi-solid-state cells was 1:1.1. The gel electrolyte used in the quasi-solid-state cells was constructed by N-acryloyl 2-glycine and liquid electrolyte with a weight ratio of 76:24. The cells were assembled in an Ar-filled glove box and tested at room temperature. The galvanostatic charge/discharge characteristics are analyzed using a LAND-CT2001 A Battery Station between 3.0 and 4.25 V using the constant current mode at 1 C-rate (1 C = 185 mAh g^{-1}) at 25 °C. Electrochemical impedance spectroscopy (EIS) is measured at different cycle number states with test frequencies from 0.1 MHz to 0.1 Hz at an Autolab electrochemical workstation.

Result and discussion

To evaluate the electrochemical performance of pristine NCM811 and NCM811-AlF_3, half cells were constructed using two NCM811, a lithium metal anode, and a liquid electrolyte, and the charge–discharge curves were tested at room temperature and a current density of 1.0 C. The result showed that the initial capacity of pristine NCM811 was 139.8 mAh g^{-1}, which is similar with the capacity of NCM811 reported in some published literature [26, 27]. After coating with AlF_3, the initial capacity was increased to 154.2 mAh g^{-1}. The cycle performance testing (Fig. 1a) showed that the capacity of NCM811-AlF_3 was 119.1 mAh g^{-1} after 200 cycles, which exceeded that of pristine NCM811, demonstrating that the AlF_3 protective layer improved the stability of NCM811 during cycling. The rate capability further demonstrates the advantage of the AlF_3 coating (Fig. 1b). The cells were charged between 3.0 and 4.25 V at a current density of 18 mA g^{-1} (0.1 C) to 900 mA g^{-1} (5.0 C). NCM811-AlF_3 exhibited better rate capability than pristine NCM811. This result indicates that the rate capability of NCM811 was improved by AlF_3 protective layer modification. Figure 1c and d show the EIS of two samples recorded at different cycles. A simplified equivalent circuit was used to fit the impedance spectrum. Resistance (RS) represents the uncompensated ohmic resistance. The first pair of resistors (Rf) and constant phase elements (CPE) represent the migration of lithium through the surface film region. The second pair of resistors (Rct) and CPE represent the charge transfer resistance and double-layer capacitance, respectively. Warburg impedance (WS) represents the solid-state diffusion reaction. The complex nonlinear least square fitting method is used to determine the electrical parameters in the equivalent circuit. The intermediate-frequency semicircle was due to the resistance of the charge transfer process at the electrode/electrolyte interface. The low-frequency tail is related to the diffusion process of lithium-ion in the cathode. The impedance of pristine NCM811 was lower than that of NCM811-AlF_3 before cycling. The higher impedance of NCM811-AlF_3 than that of pristine NCM811 was due to the AlF_3 layer. The impedances of the two samples were all increased in the cycling process, while NCM811-AlF_3 showed a lesser increment. The impedance of NCM811-AlF_3 was lower than that of pristine NCM811 after 200 cycles, illustrating that AlF_3 treatment by ALD helped prevent the increase in interfacial resistance (Table 1). For NCM811, the initial R_f and R_{ct} were 5.61 and 8.85 Ω, respectively, and after 200 cycles of charge–discharge, the R_f and R_{ct} increased to 20.46 and 15.10 Ω, respectively; for the NCM811-AlF_3, the initial R_f and R_{ct} were 3.40 and 13.26 Ω, respectively, and after 200 cycles of charge–discharge, the R_f and R_{ct} increased to 10.25

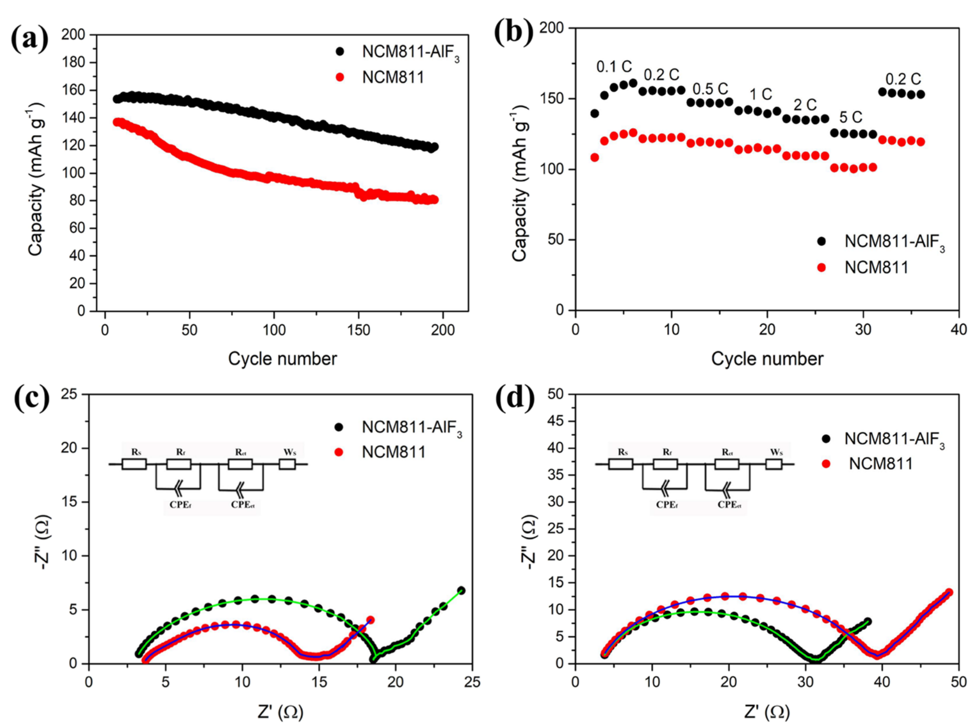

Fig. 1 Cycling curves (**a**) and rate capability (**b**) of pristine NCM811 and NCM811-AlF_3 at 1.0 C in half cells and EIS data of pristine NCM811 and NCM811-AlF_3 before cycling (**c**) and after 200 cycles (**d**)

Table 1 Simulated equivalent circuit result of pristine NCM811 and NCM811-AlF_3

	R_s	R_f	R_{ct}	CPE_f	CPE_{ct}	W_s
NCM811	2.63 Ω	5.61 Ω	8.85 Ω	2.46×10^{-5} μF	4.72×10^{-2} μF	23.48 Ω/cm^2
NCM811-AlF_3	3.12 Ω	3.40 Ω	13.26 Ω	2.82×10^{-6} μF	6.88×10^{-3} μF	35.16 Ω/cm^2
200 cycle NCM811	2.78 Ω	20.46 Ω	15.10 Ω	3.72×10^{-6} μF	0.59×10^{-3} μF	40.90 Ω/cm^2
200 cycle NCM811-AlF_3	2.83 Ω	10.25 Ω	16.82 Ω	1.75×10^{-5} μF	0.76×10^{-3} μF	18.87 Ω/cm^2

and 16.82 Ω, respectively. The improvement in interfacial resistance was mainly attributed to the suppression of direct contact between NCM811 and the electrolyte by the AlF_3 layer [28].

Figure 2a and b show the XRD patterns of pristine NCM811 and NCM811-AlF_3. The diffraction peaks yielded a well-defined hexagonal α-$NaFeO_2$-type structure (space group R-3 m) [29]. Sharp diffraction peaks and distinct splitting of (006)/(102) and (108)/(110) peaks were observed in the two samples, indicating that both samples have a typical layered crystalline structure [30]. Therefore, the XRD results suggest that the AlF_3 layer did not affect the original structure and crystallinity of NCM811. A cationic mixture of NCM811 due to the approximately similar ionic radius of Ni^{2+} and Li^+ (0.69 and 0.76 Å, respectively) negatively affected the cyclic stability. Therefore, the elimination of the cationic mixture was crucial. Rietveld refinement was adopted to explore the effect of the AlF_3 protective layer on the cationic mixture of NCM811. The Rietveld refinement depicted in Fig. 2a and b revealed that the crystal structure of NCM811 was similar to that of pristine NCM811, indicating that the protective layer did not affect the crystal structure of NCM811. The refinement results listed in Table 2 show that the cation mixture of these two samples was 3.5% and 2%, respectively, indicating that AlF_3 coating helped reduce the cationic mixing. In addition, the intensity ratios of (003) and (104) peaks representing the transition metal layer and the lithium-ion layer of the transition metal layer can intuitively reflect the degree of cationic mixing. Table 2 shows that the ratio I(003)/I(104) of NCM811 and NCM811-AlF_3 is 1.52 and 1.68, respectively. The result of Rietveld refinement demonstrated that the AlF_3 protective layer modified on the surface of NCM811 by ALD treatment could effectively suppress the cationic mixing of Ni^{2+} and Li^+.

Figure 2c and f show the HR-TEM and selected area electron diffraction (SAED) images for pristine and AlF_3-coated NCM811 (Fig. 2c and f). Partial particles on the surface were spontaneously converted to rocksalt in Fig. 2c, with a lattice spacing of 1.25 Å, and Fig. 2f shows the NCM811 of hexagonal-layered structure after coating. Notably, the

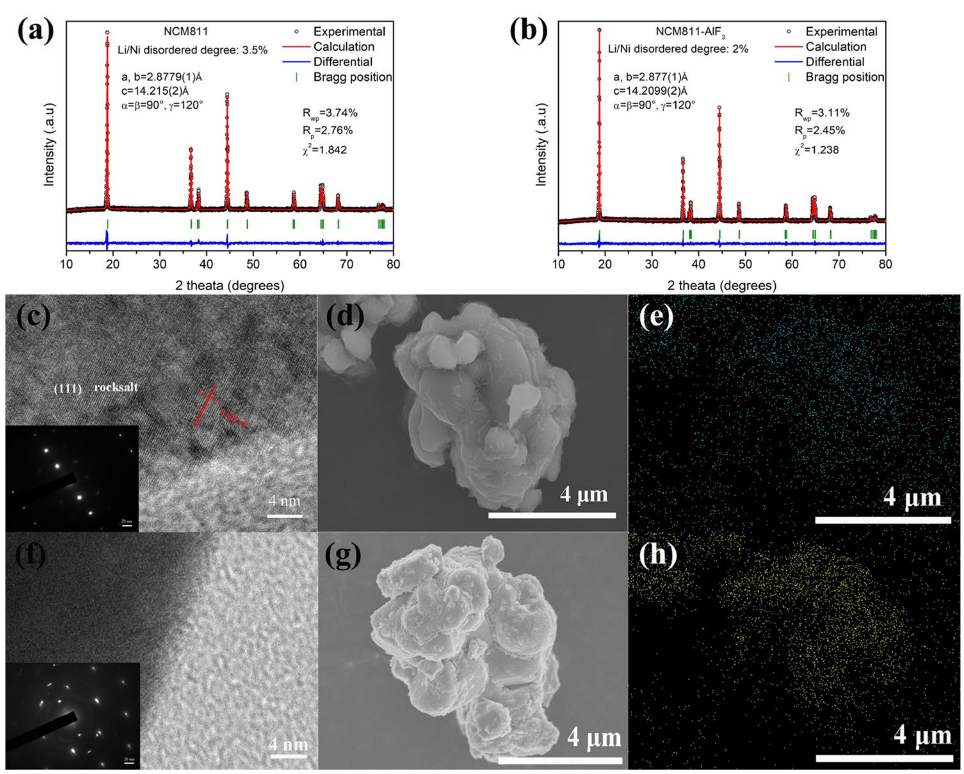

Fig. 2 XRD pattern and Rietveld refinement of **a** pristine NCM811; **b** NCM811-AlF_3. The black circle is experimental XRD data and the solid red line is calculated pattern from Rietveld refinement; TEM images of **c** pristine NCM811 and **f** NCM811-AlF_3-coated cathode material particle. Insets in **c** and **f** are the corresponding SAED paterns. **g** SEM image with pristine NCM811. **d** SEM image with EDX mapping of **e** Al and **h** F elements of NCM811-AlF_3

Table 2 Rietveld refinement result of pristine NCM811 and NCM811-AlF_3

	a (Å)	*b* (Å)	*c* (Å)	*c*/*a*	*I*(003)/*I*(104)	Li/Ni disorder
NCM811	2.878(1)	2.876(1)	14.215(2)	4.939	1.52	3.5%
NCM811-AlF_3	2.877(1)	2.877(1)	14.210(2)	4.939	1.68	2.0%

pristine particle and NCM811-AlF_3 present a uniform and regular distribution from bulk to surface before the electrochemical operation. (Fig. 2c and f). Figure 2g shows that the SEM image of pristine NCM811 has a spherical structure with several agglomerated primary particles, with an NCM811 particle size of 3–4 µm. Figure 2d shows that morphology was unaffected by AlF_3 coating. The EDX results indicate that the sAlF_3 protective layer is evenly distributed on the surface of NCM811 without any obvious coating trace (Fig. 2e and h).

The valence state and distribution of Al and F elements were tested by XPS. The XPS results show that Al 2p and F 1 s spectra were detected in AlF_3-coated NCM811, validating the presence of the AlF_3 protective layer, as shown in Fig. 3a and b. However, Ni^{3+} is an unstable state that is easily reduced to Ni^{2+}, resulting in the cation mixture [31]. Figure 3c and d show the Ni 2p3/2 spectra of NCM811 and AlF_3-coated NCM811 composed of Ni^{2+} and Ni^{3+} at 854.5 and 855.8 eV, respectively, as well as the satellite peak located at 860.7 eV. The deconvoluted Ni 2p peaks indicated the coexistence of Ni^{2+} and Ni^{3+} in the two samples; moreover, the NCM811-AlF_3 has a higher atomic percentage of Ni^{3+} ions (84%) than the pristine NCM811 (80%) according to the peak area ratio of Ni^{3+} and Ni^{2+}. The higher Ni^{3+}/Ni^{2+} ratio in NCM811-AlF_3 indicated that AlF_3 coating inhibited the loss of lithium from the NCM811 surface due to the

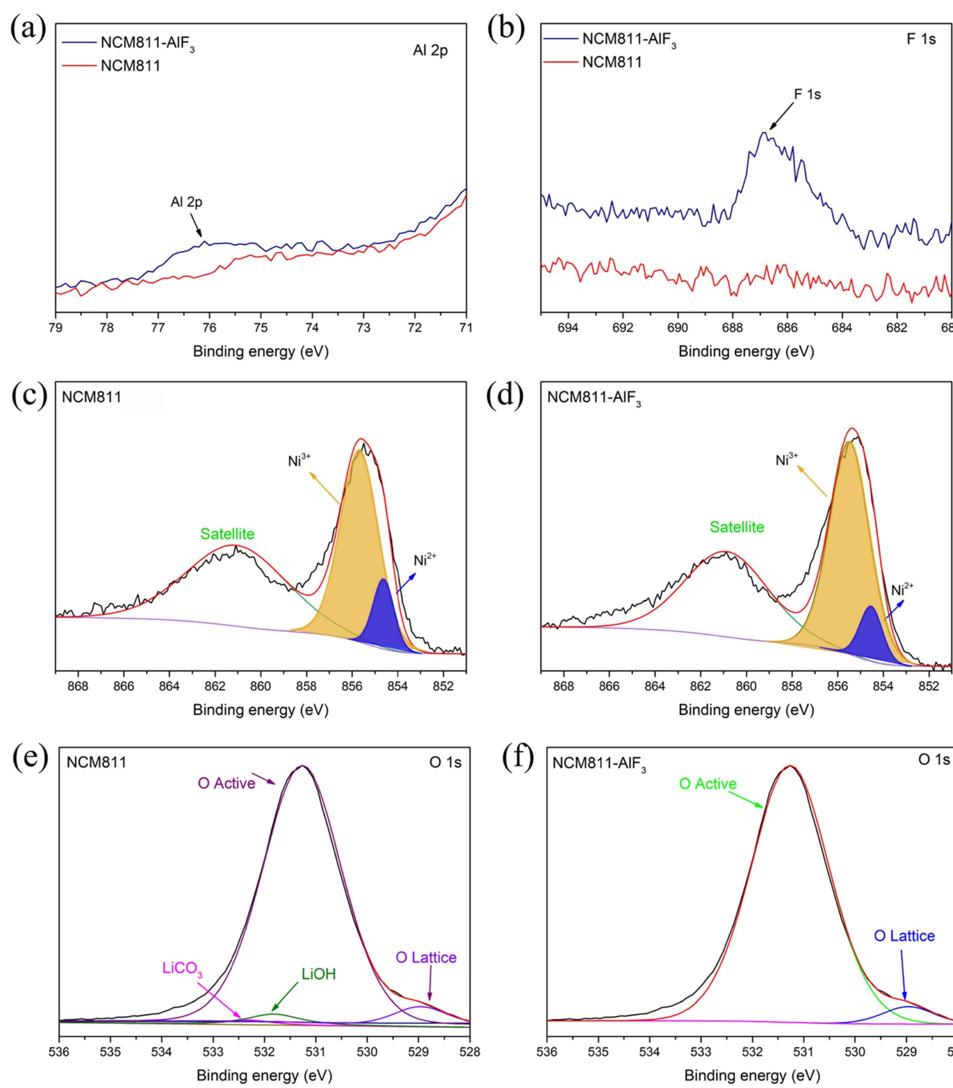

Fig. 3 XPS narrow scan spectra (**a**, **b**) Al 2p and F 1 s of pristine NCM811 and NCM811-AlF_3, (**c**, **e**) Ni 2p and O 1 s of pristine NCM811, and **d**, **f** Ni 2p and O 1 s of NCM811-AlF_3

reaction of lithium with water and carbon dioxide in the air; thus, fewer crystal defects were observed for NCM811-AlF_3, which would be beneficial for the fast insertion/extraction of lithium ions and lowering polarization resistance. Therefore, introducing the AlF_3 protective layer to the surface of NCM811 can decelerate the reduction of Ni^{3+} to Ni^{2+}, resulting in the formation of fewer crystal defects on the NCM811 surface. In-apparent peaks of Li_2CO_3 and LiOH were detected in the O 1 s spectrum of NCM811-AlF_3, whereas Li_2CO_3 and LiOH structures were found in the pristine NCM811, demonstrating that AlF_3 coating can effectively protect NCM811 from water and carbon dioxide, as shown in Fig. 3e and f. The HF precursor used during the AlF_3 ALD oxidized the surface Ni on the other side of the shield [32]. In addition, the residual alkali on the surface of NCM811 was decreased after depositing the AlF_3 layer, which reduced the generation of HF via the reaction of LiOH and $LiPF_6$, preventing NCM811 corrosion [33].

The quasi-solid-state LIBs were fabricated using graphite anode and gel polymer electrolyte with NCM811-AlF_3 and pristine NCM811, respectively. The charge–discharge curves of the quasi-solid-state LIBs were tested at room temperature at a current density of 1.0 C. The results showed that the initial capacity of NCM811-AlF_3 reached 180 mAh g^{-1}. The capacity retention of NCM811-AlF_3 was 86.5% after 500 cycles and the Coulombic efficiency was up to 99.8%. In comparison, the capacity of pristine NCM811 at the first cycle was only 148 mAh g^{-1}, and after 500 cycles, the capacity retention was 71.4% and the Coulombic efficiency was 84.5% (Fig. 4). To explore the electrochemical performance optimization mechanism of the AlF_3 protective layer, the phase, morphology, and electrochemical performance of NCM811-AlF_3 and pristine NCM811 were characterized before and after characterizing the quasi-solid pouch-cell cycling tests. XRD results showed that no significant change in the material phase was observed before and after AlF_3 coating (Fig. 5). However, the peak intensity ratio of (003)/(104) of pristine NCM811 decreased from 1.52 to 1.3 after 500 cycles, indicating that the material's lithium–nickel mixing phenomenon was aggravated after 500 cycles, whereas the (003)/(104) peak intensity ratio of NCM811-AlF_3 slightly changed from 1.68 to 1.55 after 500 cycles, indicating that the AlF_3 coating suppresses the Li/Ni mixture during cycling. Meanwhile, Fig. 5 shows that the 2θ of (003) and (104) peaks in pristine NCM811 were negatively shifted by 0.08° after 500 cycles, indicating that the interlayer spacing of NCM811 was increased after cycling due to Li loss during the charge–discharge process, resulting in the electrode material's capacity loss [34]. Compared with pristine NCM811, the 2θ of (003) and (104) peak in NCM811-AlF_3 was only negatively shifted by 0.05°, demonstrating that the AlF_3 coating decelerated Li loss during the cycling test. Therefore, AlF_3 coating could improve

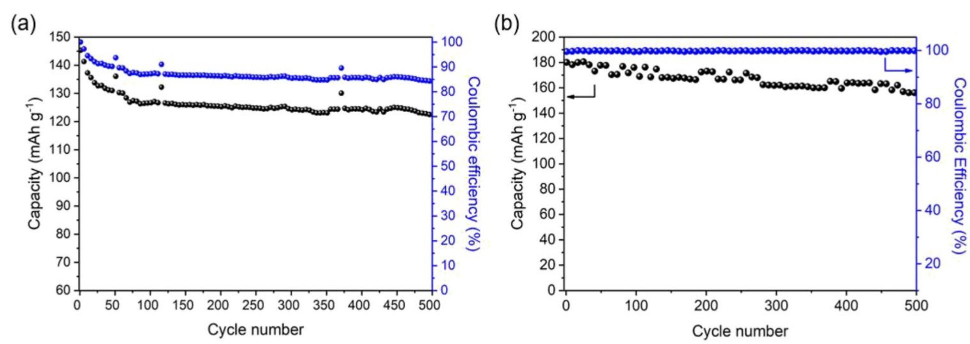

Fig. 4 Cycling curves of the **a** pristine NCM811 and **b** NCM811-AlF_3 in quansi-solid LIBs

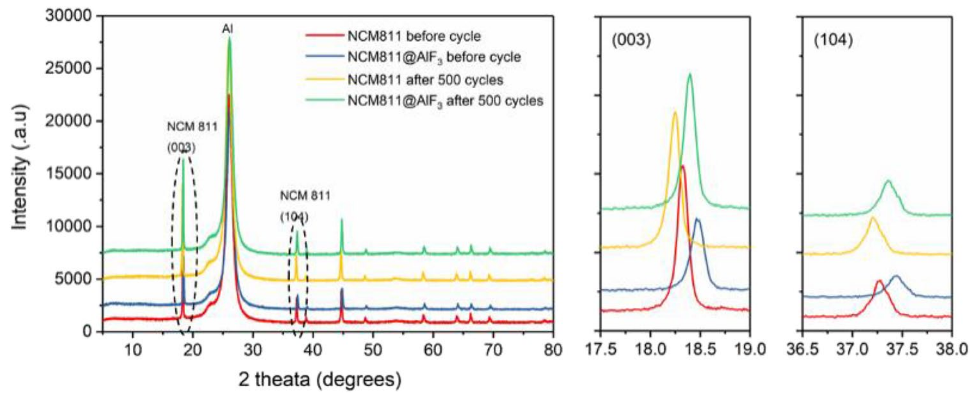

Fig. 5 XRD patterns of pristine NCM811 and NCM811-AlF_3 before and after 500 cycles in quansi-solid LIBs

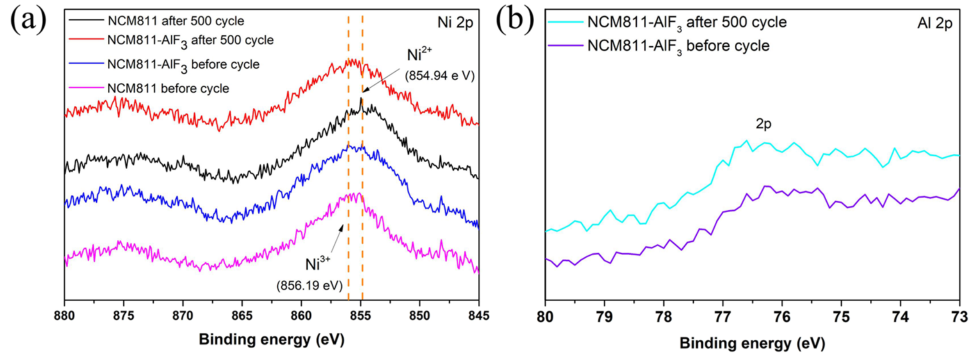

Fig. 6 XPS narrow scan spectra at **a** Ni 2p of pristine NCM811 and NCM811-AlF_3 before and after 500 cycles in quansi-solid LIBs; **b** XPS spectra et al. 2p of NCM811-AlF_3 before and after 500 cycles in quansi-solid LIBs

the structural stability of NCM811 during the charge–discharge process.

XPS analysis provides further information on the surface chemistry of the modified NCM811 sample. Figure 6 shows that the content of Ni^{3+} species in NCM811-AlF_3 increased after cycling, whereas that for pristine NCM811 decreased after 500 cycles. Similarly, the Ni 2p spectra have a slight positive shift after ALD coating and 500 cycles, demonstrating that the Ni^{3+} content was higher in the coating cathode. The transformation of the layered structure to the spinel and rock salt phases caused by side reactions during the cycle was restrained by the AlF_3 coating, which reduced the mixed arrangement degree of lithium with nickel, contributing to the stable structure during the charge–discharge process [23, 35, 36]. Therefore, AlF_3 protective layer can significantly enhance the battery performance and stability of NCM811 in quasi-solid LIBs.

Conclusion

In summary, $LiNi_{0.8}Co_{0.1}Mn_{0.1}$ (NCM811) with AlF_3 coating was synthesized by ALD and the mechanism for optimizing structural stability and electrochemical properties was systematically discussed. TEM analysis shows that the coating layer is homogeneous, with a thickness of around 1–2 nm. The results of SEM and XRD indicate that the material's morphology and structure remained unchanged after the AlF_3 coating. The AlF_3 protected layer stabilized NCM811 by preventing Li/Ni mixture, Li loss, and residual alkali generation. The initial capacity of NCM811 in a half cell with AlF_3 protection is 154.2 mAh g^{-1} at 1 C, which is higher than the 139.8 mAh g^{-1} for pristine NCM811. The capacity of NCM811 with the AlF_3 protective layer is 119.1 mAh g^{-1} after 200 cycles, which is higher than the 80.5 mAh g^{-1} for pristine NCM811. XPS analysis revealed that the HF precursor used during the AlF_3 ALD oxidized the surface Ni. In addition, the initial capacity of the full pouch quasi-solid cell using gel electrolyte at 1.0 C was significantly improved by 22%; meanwhile, the 167 mAh g^{-1} capacity was maintained after 500 cycles, which was better than that of pristine NCM811 (126 mAh g^{-1}). In addition, the side reactions in the cycle prevent the transformation of the layered structure to spinel and rock salt phases, which is beneficial to the stability of the structure in the charge–discharge process in XPS. This study shows that AlF_3 thin coating layer was an effective strategy for not only stabilizing the cathode surface but also preventing the Li/Ni mixture and Li loss during cycling. In the future, ALD coating of the surfaces of different types of high-capacity cathodes with conformal metal fluorides will be further studied.

Acknowledgements This work was sponsored in part by the National Natural Science Foundation of China (No. 51902119). The authors thank Liepu Technology Center, Sci-go Instrument Testing Platform, and Pirian Test Center for their technical support in our research by SEM, TEM and XPS characterization.

References

1. Xu GL, Liu X, Daali A, Amine R, Chen Z, Amine K (2020) Challenges and strategies to advance high-energy nickel-rich layered lithium transition metal oxide cathodes for harsh operation. J Adv Funct Mater 30(46):2004748
2. Pender JP, Jha G, Youn DH, Ziegler JM, Andoni I, Choi EJ, Heller A, Dunn BS, Weiss PS, Penner RM, Mullins CB (2020) Electrode degradation in lithium-ion batteries. J ACS Nano 14(2):1243
3. Dunn B, Kamath H, Tarascon JM (2011) Electrical energy storage for the grid: a battery of choices. Science 334(6058):928
4. Schipper F, Erickson EM, Erk C, Shin JY, Chesneau FF, Aurbach D (2016) Recent advances and remaining challenges for lithium ion battery cathodes. J Electrochem Soc 164(1):A6220
5. Kim UH, Park GT, Conlin P, Ashburn N, Cho K, Yu YS, Shapiro DA, Maglia F, Kim SJ, Lamp P, Yoon CS, Sun YK (2021) Cation ordered Ni-rich layered cathode for ultra-long battery life. Energy Environ Sci 14(3):1573
6. Phattharasupakun N, Wutthiprom J, Duangdangchote S, Sarawutanukul S, Tomon C, Duriyasart F, Tubtimkuna S, Aphirakaramwong C, Sawangphruk M (2021) Core-shell Ni-rich NMC-nanocarbon cathode from scalable solvent-free mechanofusion for high-performance 18650 Li-ion batteries. Energy Stor Mater 36:485
7. Whittingham MS (2004) Lithium batteries and cathode materials. Chem Rev 104(10):4271

8. Cao Y, Meng X, Elam JW (2016) Atomic layer deposition of LixAlyS solid-state electrolytes for stabilizing lithium-metal anodes. ChemElectroChem 3(6):858
9. Chen Z, Qin Y, Amine K, Sun YK (2010) Role of surface coating on cathode materials for lithium-ion batteries. J Mater Chem 20(36):7606
10. Yue P, Wang Z, Guo H, Xiong X, Li X (2013) A low temperature fluorine substitution on the electrochemical performance of layered $LiNi_{0.8}Co_{0.1}Mn_{0.1}O_{2-z}F_z$ cathode materials. Electrochim Acta 92:1
11. Li J, Downie LE, Ma L, Qiu W, Dahn JR (2015) Study of the failure mechanisms of $LiNi_{0.8}Mn_{0.1}Co_{0.1}O_2$ cathode material for lithium ion batteries. J Electrochem Soc 162(7):A1401
12. Haregewoin AM, Wotango AS, Hwang BJ (2016) Electrolyte additives for lithium ion battery electrodes: progress and perspectives. Energy Environ Sci 9(6):1955
13. Alvarado J, Schroeder MA, Pollard TP, Wang X, Lee JZ, Zhang M, Wynn T, Ding M, Borodin O, Meng YS, Xu K (2019) Bisalt ether electrolytes: a pathway towards lithium metal batteries with Ni-rich cathodes. Energy Environ Sci 12(2):780
14. Sun YK, Myung ST, Kim MH, Prakash J, Amine K (2005) Synthesis and characterization of $Li[(Ni_{0.8}Co_{0.1}Mn_{0.1})_{0.8}(Ni_{0.5}Mn_{0.5})_{0.2}]O_2$ with the microscale core-shell structure as the positive electrode material for lithium batteries. J Am Chem Soc 127(38):13411
15. Xiong X, Wang Z, Guo H, Zhang Q, Li X (2013) Enhanced electrochemical properties of lithium-reactive V_2O_5 coated on the $LiNi_{0.8}Co_{0.1}Mn_{0.1}O_2$ cathode material for lithium ion batteries at 60 °C. J Mater Chem A 1(4):1284
16. Wise AM, Ban C, Weker JN, Misra S, Cavanagh AS, Wu Z, Li Z, Whittingham MS, Xu K, George SM, Toney MF (2015) Effect of Al_2O_3 coating on stabilizing $LiNi_{0.4}Mn_{0.4}Co_{0.2}O_2$ cathodes. Chem Mater 27(17):6146
17. Chen Y, Zhang Y, Chen B, Wang Z, Lu C (2014) An approach to application for $LiNi_{0.6}Co_{0.2}Mn_{0.2}O_2$ cathode material at high cutoff voltage by TiO_2 coating. J Power Sources 256:20
18. Hou P, Zhang H, Zi Z, Zhang L, Xu X (2017) Core–shell and concentration-gradient cathodes prepared via co-precipitation reaction for advanced lithium-ion batteries. J Mater Chem A 5(9):4254
19. Deng S, Li X, Ren Z, Li W, Luo J, Liang J, Liang J, Banis MN, Li M, Zhao Y, Li X, Wang C, Sun Y, Sun Q, Li R, Hu Y, Huang H, Zhang L, Lu S, Luo J, Sun X (2020) Dual-functional interfaces for highly stable Ni-rich layered cathodes in sulfide all-solid-state batteries. Energy Stor Mater 27:117
20. Dong X, Yao J, Zhu W, Huang X, Kuai X, Tang J, Li X, Dai S, Shen L, Yang R, Gao L, Zhao J (2019) Enhanced high-voltage cycling stability of Ni-rich cathode materials via self-assembly of Mn-rich shells. J Mater Chem A 7(35):20262
21. Zhou Y, Lee Y, Sun H, Wallas JM, George SM, Xie M (2017) Coating solution for high-voltage cathode: AlF_3 atomic layer deposition for freestanding $LiCoO_2$ electrodes with high energy density and excellent flexibility. ACS Appl Mater Interfaces 9(11):9614
22. Sun YK, Lee MJ, Yoon CS, Hassoun J, Amine K, Scrosati B (2012) The role of AlF_3 coatings in improving electrochemical cycling of Li-enriched nickel-manganese oxide electrodes for Li-ion batteries. Adv Mater 24(9):1192
23. Wang E, Zhao Y, Xiao D, Zhang X, Wu T, Wang B, Zubair M, Li Y, Sun X, Yu H (2020) Composite nanostructure construction on the grain surface of Li-rich layered oxides. Adv Mater 32(49):e1906070
24. Shapira A, Tiurin O, Solomatin N, Auinat M, Meitav A, Ein EY (2018) Robust AlF_3 atomic layer deposition protective coating on $LiMn_{1.5}Ni_{0.5}O_4$ particles: an advanced Li-ion battery cathode material powder. ACS Appl Energy Mater 1(12):6809
25. Lee Y, DuMont JW, Cavanagh AS, George SM (2015) Atomic layer deposition of AlF_3 using trimethylaluminum and hydrogen fluoride. J Phys Chem C 119(25):14185
26. Yahya MA, Quinton LW (2022) Reduction of capacity fading in high-voltage NMC batteries with the addition of reduced graphene oxide. Materials 15:2146
27. Franziska F, Benjamin S, Anna TSF, Karin K, Sarah JD, Christoph E, Michele P, Hubert AG (2019) Capacity fading mechanisms of NCM-811 cathodes in lithium-ion batteries studied by x-ray diffraction and other diagnostics. J Electrochem Soc 166(15):A3760–A3774
28. Tan X, Zhang M, Li J, Zhang D, Yan Y, Li Z (2020) Recent progress in coatings and methods of Ni-rich $LiNi_{0.8}Co_{0.1}Mn_{0.1}O_2$ cathode materials: A short review. Ceram Int 46(14):21888
29. Chen G, Peng B, Han R, Chen N, Wang Z, Wang Q (2020) A robust carbon coating strategy toward Ni-rich lithium cathodes. Ceram Int 46(13):20985
30. Zhang Z, Zhou P, Meng H, Chen C, Cheng F, Tao Z, Chen J (2017) Amorphous $Zr(OH)_4$ coated $LiNi_{0.915}Co_{0.075}Al_{0.01}O_2$ cathode material with enhanced electrochemical performance for lithium ion batteries. J Energy Chem 26(3):481
31. David L, Dahlberg K, Mohanty D, Ruther RE, Huq A, Chi M, An SJ, Mao C, King DM, Stevenson L, Wood DL (2019) Unveiling the role of Al_2O_3 in preventing surface reconstruction during high-voltage cycling of lithium-ion batteries. ACS Appl Energy Mater 2(2):1308
32. Darapaneni P, Mane AU, Turczynski A, Elam JW (2021) Elucidating the redox behavior during atomic layer deposition on lithium-ion battery cathode materials. Chem Mater 33(20):8079
33. Li W, Erickson EM, Manthiram A (2020) High-nickel layered oxide cathodes for lithium-based automotive batteries. Nat Energy 5(1):26
34. Shi Y, Zhang M, Meng YS, Chen Z (2019) Ambient-pressure relithiation of degraded $LixNi_{0.5}Co_{0.2}Mn_{0.3}O_2 (0 < x < 1)$ via eutectic solutions for direct regeneration of lithium-ion battery cathodes. Adv Energy Mater 9(20):1900454
35. Dong S, Zhou Y, Hai C, Zeng J, Sun Y, Shen Y, Li X, Ren X, Qi G, Zhang X, Ma L (2019) Ultrathin CeO_2 coating for improved cycling and rate performance of Ni-rich layered $LiNi_{0.7}Co_{0.2}Mn_{0.1}O_2$ cathode materials. Ceram Int 45(1):144
36. He T, Lu Y, Su Y, Bao L, Tan J, Chen L, Zhang Q, Li W, Chen S, Wu F (2018) Sufficient utilization of zirconium ions to improve the structure and surface properties of nickel-rich cathode materials for lithium-ion batteries. Chemsuschem 11(10):1639

Publisher's note Springer Nature remains neutral with regard to jurisdictional claims in published maps and institutional affiliations.